

# Identification of the feature that causes the *I*-band secondary maximum of a Type Ia supernova

D. Jack,<sup>1</sup>★ E. Baron<sup>2,3</sup> and P. H. Hauschildt<sup>3</sup>

<sup>1</sup>*Departamento de Astronomía, Universidad de Guanajuato, Apartado Postal 144, 36000 Guanajuato, Mexico*

<sup>2</sup>*Homer L. Dodge Department of Physics and Astronomy, University of Oklahoma, 440 W Brooks, Norman, OK 73019-2061, USA*

<sup>3</sup>*Hamburger Sternwarte, Gojenbergsweg 112, D-21029 Hamburg, Germany*

Accepted 2015 March 3. Received 2015 February 16; in original form 2014 September 18

## ABSTRACT

We obtained a time series of spectra covering the secondary maximum in the *I* band of the bright Type Ia supernova 2014J in M82 with the TIGRE telescope. Comparing the observations with theoretical models calculated with the time dependent extension of the PHOENIX code, we identify the feature that causes the secondary maximum in the *I*-band light curve. Fe II  $3d^6(^3D)4s-3d^6(^5D)4p$  and similar high-excitation transitions produce a blended feature at  $\sim 7500$  Å, which causes the rise of the light curve towards the secondary maximum. The series of observed spectra of SN 2014J and archival data of SN 2011fe confirm this conclusion. We further studied the plateau phase of the *R*-band light curve of SN 2014J and searched for features which contribute to the flux. The theoretical models do not clearly indicate a new feature that may cause the *R*-band plateau phase. However, Co II features in the range of 6500–7000 Å and the Fe II feature of the *I* band are clearly seen in the theoretical spectra, but do not appear to provide all of the flux necessary for the *R*-band plateau.

**Key words:** radiative transfer – supernovae: general – supernovae: individual: SN 2014J.

## 1 INTRODUCTION

The light curves of Type Ia supernovae (SNe Ia) are of general interest, in particular for applications in cosmology. The optical light curves of SNe Ia admit a light-curve shape relation (Phillips 1993; Riess, Press & Kirshner 1996; Phillips et al. 1999; Goldhaber et al. 2001) which allows them to be used as ‘correctable candles’ and hence, their distances can be determined from the observed photometry. The underlying physical explanation for the light-curve shape relation is that the total  $^{56}\text{Ni}$  mass produced in the explosion determines to first order the temperature and thus, more  $^{56}\text{Ni}$  leads to higher temperatures, which leads to higher opacities, increasing the diffusion time (Khokhlov, Müller & Höflich 1993; Höflich, Khokhlov & Wheeler 1995; Nugent et al. 1995; Pinto & Eastman 2000a,b; Mazzali et al. 2001; Pinto & Eastman 2001). It has been questioned whether the primary effect of the  $^{56}\text{Ni}$  mass is on the diffusion time or rather on the colour evolution of the spectra (Kasen & Woosley 2007), but the ultimate source for the observed luminosity of an SN Ia is the decay of  $^{56}\text{Ni}$ , and thus to zero order the luminosity should be correlated with the mass of  $^{56}\text{Ni}$ . Using the light curves of SNe Ia for distance measurements led us to the discovery of the phenomenon that the Universe’s expansion is accelerated, i.e. the discovery of the dark energy (Riess et al. 1998; Perlmutter et al.

1999). The nature of the dark energy is of fundamental importance for cosmology.

Many physical details of SN Ia events are still not fully understood (see Hillebrandt & Niemeyer 2000; Parrent, Friesen & Parthasarathy 2014, for reviews). One of the most important open questions is the nature of the progenitor(s) of SN Ia explosions. The progenitor is believed to be a CO white dwarf in a binary system. Its companion star could be a main-sequence star, an evolved star, or another white dwarf. The primary white dwarf grows in mass via accretion, which can be slow in the Chandrasekhar-mass scenario, or rapid in scenarios that involve the merging of two white dwarfs (see Maoz, Mannucci & Nelemans 2014; Levanon, Soker & García-Berro 2015, for reviews of the suggested possibilities). In fact, SNe Ia may come from a variety of progenitor systems, and detailed observations of nearby SNe Ia may lead to the understanding of the nature of these progenitor systems (Nugent et al. 2011; Dilday et al. 2012). There is further ongoing discussion about the explosion mechanism of SNe Ia. An instantaneous detonation in Chandrasekhar-mass WDs has been ruled out, because it fails to produce intermediate mass elements (IME), which are observed in the spectra of SNe Ia (Arnett 1969). In sub-Chandrasekhar-mass WDs an instantaneous detonation can produce IME due to the lower central densities (Shigeyama et al. 1992; Sim et al. 2010). However, the mass of the WD is rather tightly constrained to produce both iron group elements and IME and the low densities will not produce observed stable iron group elements. Several different explosion models such as a pure

\* E-mail: dennis@astro.ugto.mx

deflagration, delayed detonations, gravitationally confined detonations, violent mergers, and collisions have been suggested (Nomoto 1984; Khokhlov 1991; Plewa, Calder & Lamb 2004; Jordan et al. 2008, 2012; Rosswog et al. 2009; Pakmor et al. 2012, 2013; Kushnir et al. 2013; Long et al. 2014), which could explain the appearance of the IME observed in SN Ia spectra. To understand the physical processes in an SN Ia further, different numerical codes have been developed and used to model the spectra and light curves of SNe Ia (Branch et al. 1985; Mazzali & Lucy 1993; Höflich 2003; Kasen, Thomas & Nugent 2006; Dessart & Hillier 2010; Jack, Hauschildt & Baron 2011; Sim et al. 2013; Maeda, Kutsuna & Shigeyama 2014; Wollaeger & van Rossum 2014).

We focus here on the light curves in the near-infrared wavelength region. The light curves of the near-infrared bands *I*, *J*, *H*, and *K* very often show a secondary maximum (Elias et al. 1981; Höflich et al. 2002). In his detailed study of near-infrared light curves of SNe Ia, Kasen (2006) showed that the secondary maxima are caused by the recombination of iron peak elements, which comes from a drastic opacity change between ionization stages III to II of the iron elements. This observation has been confirmed with other theoretical radiative transfer calculations (Gall et al. 2012; Jack, Hauschildt & Baron 2012; Dessart et al. 2014). Jack et al. (2012) were able to assign specific features of Fe II and Co II that cause the individual secondary maxima in the *I*, *J*, *H*, and *K* bands. However, their investigation was based only on theoretical light-curve calculations. Dessart et al. (2014) found that [Co II] lines play a strong role, but this result has not been confirmed in other calculations and may be due to the way that levels and superlevels are coupled in their approximations.

In this work, we will present observational evidence that an Fe II feature, produced by a blend of Fe II lines, causes the secondary maximum in the *I* band and additionally, we present an investigation of the plateau phase of the *R*-band light curve. In Section 2, we present the details of the observations of SN 2014J and describe the methods used to calculate the theoretical light curves with the PHOENIX code. In Section 3, we present the results obtained for the secondary maximum in the *I* band and the plateau phase of the *R* band.

## 2 METHODS

We obtained a time series of observations of high-resolution spectra of the bright SN Ia, 2014J in M82 with the TIGRE telescope. We fitted the model light curves calculated with the PHOENIX code to the observed light curves in the near-infrared *I* and *R* bands. The observed and theoretical spectra are then compared to determine the features that cause the secondary maximum in the *I* band and the plateau phase in the *R* band.

SN 2014J was discovered by Fossey et al. (2014) in the nearby galaxy M82 approximately 1 week after explosion. We use for the explosion time January 14.75 UT as found by Zheng et al. (2014).

### 2.1 Observations

We observed SN 2014J in M82 with the TIGRE telescope situated in Central Mexico close to the city of Guanajuato (Schmitt et al. 2014). The telescope TIGRE is a 1.2-m mirror telescope that operates completely robotically. Its original design was to monitor the stellar activity of solar-like stars, but other observational campaigns are also feasible. The TIGRE telescope is equipped with the HEROS (Heidelberg Extended Range Optical Spectrograph) spectrograph, which has a high resolution  $R \sim 20\,000$  and covers the wavelength

range from about 3800 Å to about 8800 Å. The spectrum is divided into two channels (red and blue). The data reduction pipeline is also fully automatic.

Beginning with the first observation during the night of 2014 January 23, we were able to observe a spectrum of SN 2014J in M82 almost every night following the discovery. See Jack et al. (2015) for a complete presentation of the time series of SN 2014J spectra observed with the TIGRE telescope. We used an exposure time of 3 h for every observed spectrum. The spectra were obtained with the full spectral resolution  $R \sim 20\,000$ . Since a supernova spectrum shows only very broad features and such a high resolution is not necessarily required, we binned the spectrum down to a resolution of 10 Å. The binning significantly improves the signal-to-noise ratio. For this work, we are interested in the near-infrared wavelength range, so that we will only use the spectra of the red channel (5800–8800 Å). SN 2014J showed significant reddening so that the obtained spectra in the blue channel (3800–5800 Å) observed at such high resolution have a much lower signal to noise.

### 2.2 Theoretical light curves

In order to model the theoretical light curves in different bands of SN 2014J, we used the time dependent extension of the PHOENIX code as described in detail in Jack, Hauschildt & Baron (2009) and Jack et al. (2011). The code follows the evolution of the supernova envelope after the explosion enforcing energy conservation. This includes energy deposition due to  $\gamma$ -rays from the radioactive decay of  $^{56}\text{Ni}$  and  $^{56}\text{Co}$ . Cooling due to the adiabatic expansion of the envelope, which is assumed to be homologous, is also included. For the transport of energy by radiation throughout the envelope, we solve the spherically symmetric special relativistic radiative transfer equation (Hauschildt 1992; Hauschildt & Baron 1999). The envelope was divided into 128 layers. About 1000 time steps are performed for each point in the light curve. We usually calculate a point in the light curve every 1 or 2 d. All light curves have been calculated assuming local thermodynamic equilibrium (LTE) and using about 2000 wavelength points. The final spectra presented in this work have been calculated using a higher resolution of about 20 000 wavelength points. PHOENIX uses the update Kurucz data base<sup>1</sup> which contains about 80 million atomic line transition. For the initial input structure, we used the results of the W7 deflagration model (Nomoto 1984), which also includes the specific non-homogeneous abundances.

In this work, we focus on the secondary maxima in the near-infrared wavelength region. We seek to obtain the best fit to the individual observed light curves of SN 2014J in the respective bands. As described in Jack et al. (2012), with the above assumptions, it is necessary to vary the equivalent two-level atom thermalization parameter when solving the radiative transfer problem. The source function of the radiative transfer equation including scattering for an equivalent two level atom can be written as

$$S_\lambda = (1 - \epsilon_\lambda)J_\lambda + \epsilon_\lambda B_\lambda. \quad (1)$$

Here,  $S_\lambda$  is the source function,  $B_\lambda$  is the Planck function, and  $J_\lambda$  is the mean intensity. All these quantities are wavelength dependent. For the LTE PHOENIX calculations, it is possible to set a wavelength independent factor  $\epsilon = \epsilon_\lambda = \text{constant}$  to approximate LTE line scattering over the whole wavelength range. We use this method here for computational expediency. Since the SN Ia envelope becomes

<sup>1</sup> <http://kurucz.harvard.edu/linelists/gfall/>

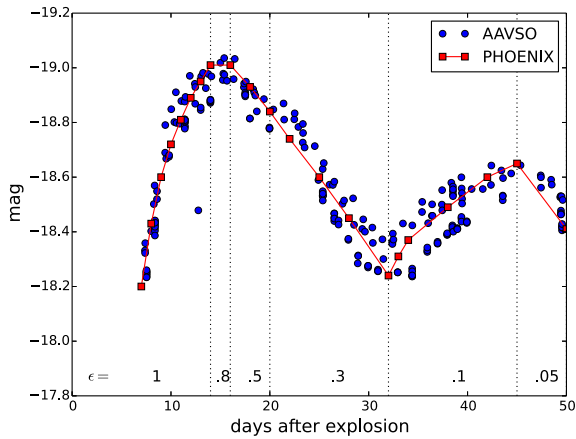


**Figure 1.** The circles represent the dereddened AAVSO observed light curve in absolute magnitude of SN 2014J in the *I* band. The solid line shows the best fit obtained from PHOENIX models. The values for  $\epsilon$  are indicated along the bottom of the plot and the vertical dotted lines demarcate the range.

thinner during its free expansion phase, scattering becomes more and more important, and the thermalization parameter  $\epsilon$  decreases. Applying this method of a decreasing thermalization parameter, we obtained fits to the observed light curves of SN 2014J.

### 3 SECONDARY MAXIMUM

We compare the spectra of SN 2014J observed with the TIGRE telescope with the theoretical spectra calculated with PHOENIX focusing on the secondary maximum of the *I*-band light curve and the plateau phase observed in the *R* band. All observed spectra and light curves have been dereddened with the values  $E(B - V) = 1.33$  and  $R_V = 1.3$  found by Amanullah et al. (2014) in their study of the extinction law of SN 2014J.

#### 3.1 *I* band

We obtained a time series of spectra of SN 2014J during the rise of the light curve towards the secondary maximum in the *I* band. Unfortunately, the HEROS spectrograph does not cover the whole range of the *I*-band filter, meaning that we could not reconstruct a light curve from our observed spectra. Therefore, we used the observed light curve of the AAVSO data base<sup>2</sup> to find the best fit of the model light curve calculated with PHOENIX. As described above, we varied the thermalization parameter  $\epsilon$  to obtain the best fit to the observed light curve in the *I* band. Although this is not a physically correct method to calculate a light curve, the overall trend of a decreasing  $\epsilon$  is physically motivated. However, the goal here is to use this fit to study the spectral evolution of an SN Ia towards the secondary maximum.

In Fig. 1, the filled circles represent the light curve of SN 2014J in the *I* band obtained from AAVSO observation data. The observed light curve has been dereddened. We also plotted the AAVSO light curve in absolute magnitude using the distance of 3.5 Mpc to M82, which results in a distance modulus of 27.7 mag, which is comparable with the value of 27.6 mag found by Foley et al. (2014). The solid line represents the best fit of the theoretical light curve calculated with PHOENIX models. As stated above, the models were

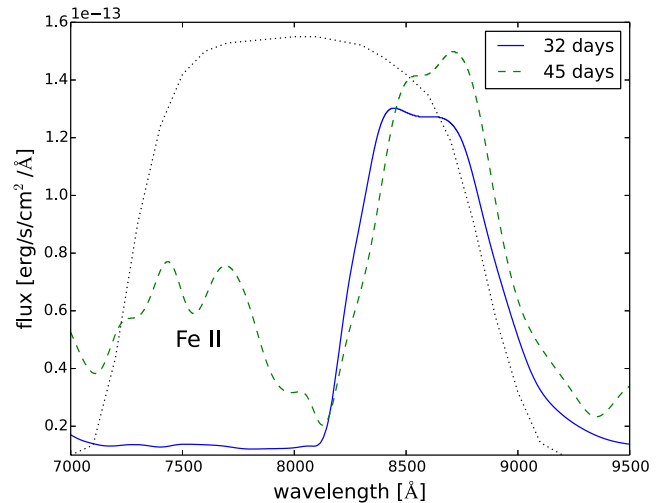


**Figure 2.** Theoretical spectra at different epochs after the explosion calculated with PHOENIX. At  $\sim 7500$  Å, a new feature of blended Fe II lines appears and causes the secondary maximum. The dotted line indicates the *I*-band filter response.

calculated with different values of  $\epsilon$  for different epochs. This causes the kinks in the model light curve. The rise towards the secondary maximum is clearly visible and starts around 32 d after the explosion. The secondary maximum is reached at around 45 d. These are the epochs that are interesting for studying the spectral evolution and identifying the feature that causes this secondary maximum.

In Fig. 2, we show a plot of the theoretical spectra calculated with PHOENIX at different epochs obtained from the best fit to the observed light curve. The spectra are shown in flux received at Earth if the models would be at the distance of SN 2011fe (6.6 Mpc) to be able to compare the fluxes directly. The dotted line shows the *I*-band filter response. At that epoch the spectrum does not show many clear features. The brightness decreases after the *I* maximum. The Ca II IR triplet feature at 8500–9000 Å becomes prominent. However, this feature, does not show a change in brightness during the rise to the secondary maximum. From the beginning of the rise (32 d) up to the secondary maximum (45 d) there appears a new feature of Fe II at a wavelength of  $\sim 7500$  Å. In Fe II there are numerous transitions from relatively high excited states in this wavelength region, for example transitions from  $3d^6(^3D)4s - 3d^6(^5D)4p$ ,  $3d^5(^4P)4s4p(^3P^o) - 3d^6(^5D)6s$ , and similar transitions, which have Einstein coefficient  $A_{21}$  values  $> 1 \times 10^7 \text{ s}^{-1}$ . Thus, this feature causes the observed secondary maximum in the *I* band of SNe Ia.

The observed spectra also clearly show the appearance of the Fe II feature mentioned above. Fig. 3 shows two observed spectra of SN 2014J in the same wavelength range as was used for the theoretical spectra in Fig. 2. The dotted line represents the *I*-band filter response. The spectrum from February 16 was taken directly before the beginning of the rise towards the secondary maximum. The spectrum from the March 1 was observed during the secondary maximum. These observed spectra correspond to the theoretical spectra of day 32 and day 45 in Fig. 2. The feature of Fe II at around 7500 Å also appears in the observed spectra. Note that there is a strong telluric absorption feature around 7600 Å, which contaminates the spectrum in this region. However, we can clearly confirm that this Fe II feature actually causes the secondary maximum in the *I* band of SN 2014J, and thus, it is likely the cause in most SNe Ia.

Since our observed spectra of SN 2014J do not cover the whole wavelength range of the *I* band, we used archival data to obtain

<sup>2</sup> [www.aavso.org](http://www.aavso.org)

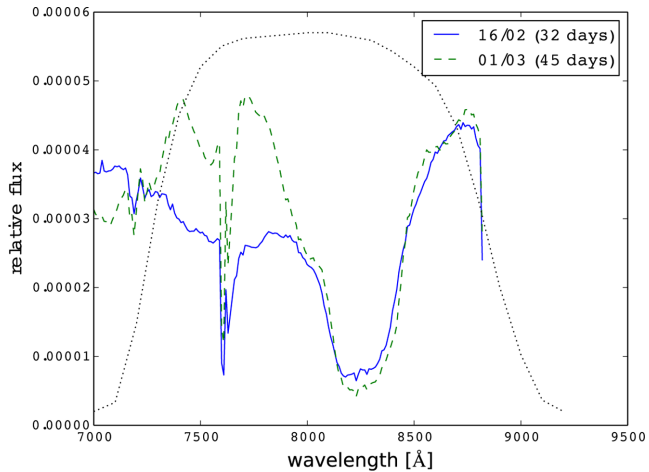


**Figure 3.** Spectra of SN 2014J observed on two different days before and during the secondary maximum. The appearance of the feature of blended Fe II lines can be seen in the observations at  $\sim 7500$  Å as well. The dotted line represents the *I*-band filter function.

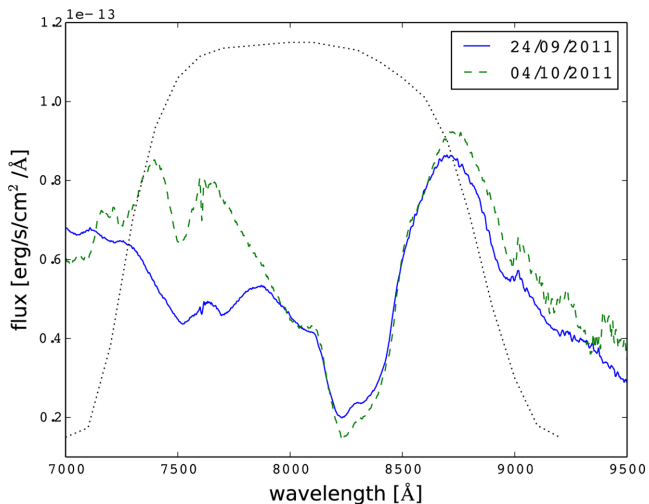


**Figure 4.** Spectra of SN 2011fe observed. The appearance of the feature of blended Fe II lines can be seen in the observations at  $\sim 7500$  Å as well. The dotted line represents the *I*-band filter function.

additional evidence that the Fe II feature causes the secondary maximum.

In Fig. 4, we show two spectra of SN 2011fe. The spectra were observed by the Nearby Supernova Factory (Pereira et al. 2013) in a time series of spectra. The spectrum from the 2011 September 24 coincides with the minimum before the rise towards the secondary maximum in the *I* band. The secondary maximum was observed around the 2011 October 8. Unfortunately, there does not exist a spectrum of that day. Therefore, we used the spectrum of the October 4. In the plot one can clearly see that a feature around  $7500$  Å arises. This gives more observational evidence that this Fe II feature causes the secondary maximum in the *I* band of SNe Ia.

### 3.2 *R* band

The light curve of a typical SNe Ia in the *R* band does not show a secondary maximum, but usually a short plateau phase. Since all other light curves in the optical wavelength range show a steady decline after maximum light, there should also be a feature that

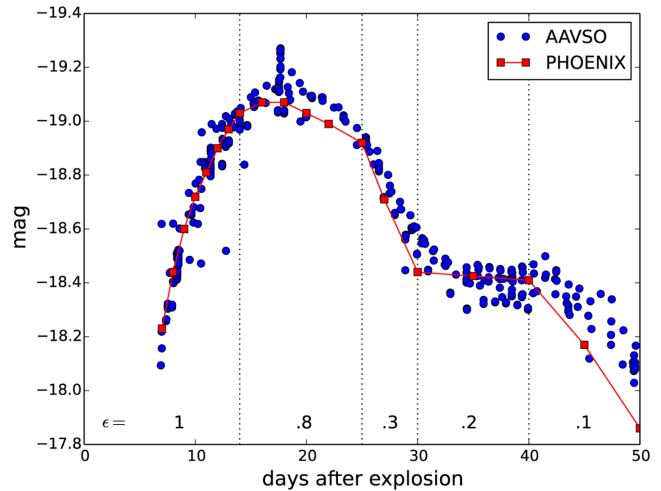


**Figure 5.** The circles represent the dereddened AAVSO observed light curve in absolute magnitude of SN 2014J in the *R* band. The solid line shows the best fit obtained from PHOENIX models. The values for  $\epsilon$  are indicated along the bottom of the plot and the vertical dotted lines demarcate the range.

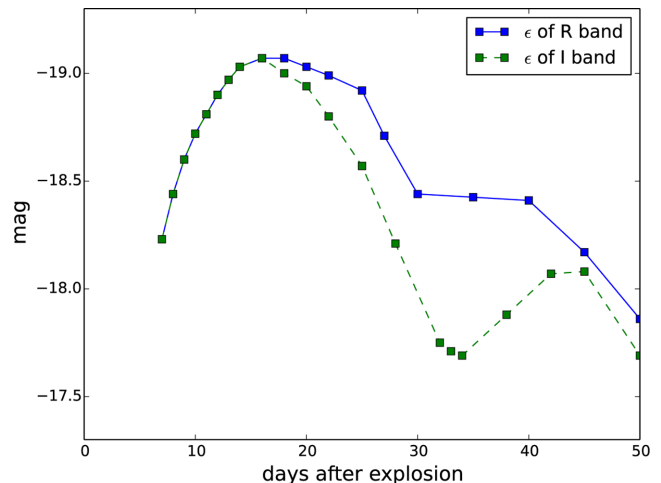


**Figure 6.** Here we show the PHOENIX *R*-band light curve calculated with the  $\epsilon$  values for the *I* band and *R* band.

causes the effective *R*-band photosphere to ‘hang up’. We used the same method to identify this feature as in the study of the *I*-band secondary maximum. Using a varying line thermalization parameter  $\epsilon$ , we obtained a best fit to the observed (dereddened) *R*-band light curve of SN 2014J.

In Fig. 5, the filled circles show the observed AAVSO light curve in the *R* band. Between about 30 and 40 d after explosion the *R*-band light curve of SN 2014J shows a short plateau phase, which we also modelled with the theoretical light curve of PHOENIX. The solid line represents the best fit obtained from PHOENIX models by varying the thermalization parameter. Note that the variations of  $\epsilon$  are slightly different from those used to compute the *I*-band light curve. The differences, while small, represent a limitation in our modelling approach. However, the overall trend of a decreasing  $\epsilon$  is the same for all near-infrared bands. Scattering becomes more and more important as the SN Ia envelope expands.

In Fig. 6, we compare the *R*-band light curves that have been calculated using the values for  $\epsilon$  used for the *R* band and for the *I* band. One can see some clear differences during the phase of the

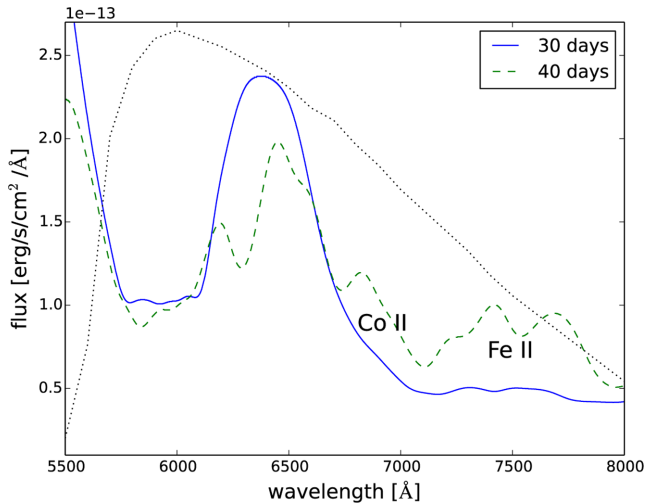


**Figure 7.** Spectra of the best fit to the *R*-band light curve. Two features of blended Co II lines and blended Fe II lines contribute to the flux that causes the *R*-band plateau phase. The dotted line represents the *R*-band filter function. The model luminosity has been scaled by the distance to SN 2011fe.

minimum before the plateau phase. However, since  $\epsilon$  is wavelength dependent, it is not possible to distinguish between a possible inaccuracy of the models or a real difference in the value of  $\epsilon$  for the different wavelength regions. We then studied the spectral evolution during this observed plateau phase. In Fig. 7, we show the theoretical spectra calculated with PHOENIX at the beginning of the plateau phase (30 d) and at the end of the *R*-band plateau (40 d). The dotted line represents the *R*-band filter function. After the *R* maximum (16 d), the brightness decreases in the whole wavelength range. At 30 d, which marks the beginning of the plateau phase, the characteristic P-Cygni Si II feature around 6000 to 6500 Å strengthens. This feature changes between 30 and 40 d during the plateau phase. However, the contribution of this feature to the brightness in the *R* band decreases and can, therefore, not cause the plateau phase. In the models, blends of high-excitation Co II lines appear in the wavelength region 6500–7000 Å; however, the total flux in the models is not large enough to produce the observed plateau. The feature of Fe II at 7500 Å that causes the secondary maximum in the *I* band is also present in the *R*-band filter, but again the filter sensitivity is falling off here so the total flux is not large enough to produce the observed plateau.

While nickel holes are seen in SNe Ia (Fesen et al. 2007), the nickel hole in W7 is too large to be compatible with galactic nucleosynthesis and thus, the centre of W7 has too much stable Ni and Fe, which will reduce the total amount of Co. However, the Co II lines seen in the models are not easily identified in the observations (see below).

Fig. 8 shows the observed spectra of SN 2014J in the *R* band using the same wavelength range as for the theoretical spectra of Fig. 7. The dotted line once again represents the *R*-band filter function. We plotted the spectrum from February 14, which corresponds to the beginning of the plateau phase (30 d). The end of the plateau phase at 40 d is represented by the observed spectrum from the February 24. One can clearly see the change of the expansion velocity of the characteristic Si II feature as the photosphere moves inwards. There is no clear feature arising in the *R* band that obviously causes the short plateau phase. Of course, the Fe II feature at around 7500 Å also contributes somewhat to the light curve in the *R* band. As discussed

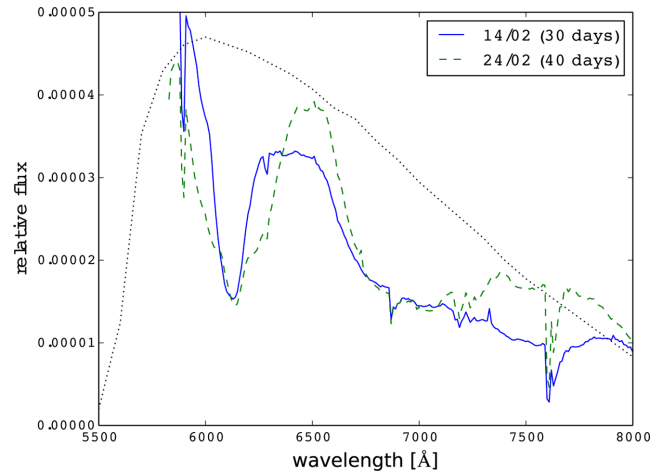


**Figure 8.** Spectra of SN 2014J observed on two different days at the beginning and the end of the *R*-band plateau phase. The Fe II features is clearly visible while the Co II feature of the models has not been identified. The dotted line represents the *R*-band filter function.

above Co II lines in the 6500–7000 Å range are seen in the models, but their signatures are not strong in the observed spectra.

#### 4 CONCLUSIONS

We observed a time series of spectra of the nearby SNe Ia 2014J in M82 with the TIGRE telescope. This time series also covered the secondary maximum in the *I* band and the plateau phase in the *R* band. We calculated the respective theoretical light curves with the time-dependent extension of the PHOENIX code by varying the line thermalization parameter to obtain a best fit to the observed light curves. For the *I*-band light curve of SN 2014J, we find that the secondary maximum is caused by a blend of Fe II high-excitation lines because of the recombination of iron peak elements from ionization stage III to stage II. This confirms previous work studying near-infrared light curves of SNe Ia (Kasen 2006; Jack et al. 2012; Dessart et al. 2014). Studying the spectral evolution of SN 2014J, we find observational evidence that the Fe II feature at around 7500 Å causes the secondary maximum in the *I* band. While W7 is only a parametrized model of a real SN Ia, the interior composition is fairly generic due to the nuclear physics and thus, our conclusion should be fairly general. However, the details are a bit more complicated, and recent explosion calculations show quite some diversity in the ejected material (Woosley & Kasen 2011; Fink et al. 2014; Moll et al. 2014).

As far as we know, there exists no detailed study of the *R*-band light curves of SNe Ia. We observed SN 2014J, and it – like most other SNe Ia – shows a short plateau phase in the *R* band between 30 and 40 d after the explosion. We reproduced the observed light curve with our PHOENIX models to be able to identify the feature that causes this short plateau phase. Co II lines in the range 6500–7000 Å do increase in flux in the models, and the Fe II lines to the red may also contribute somewhat, but the total flux from these features does not appear to be large enough in the models and the Co II signatures are not clearly seen in the observations.

For future work, it will be very interesting to study the spectral evolution of an SN Ia in the other near-infrared bands *J*, *H*, *Y*, and *K*. With this one might be able to identify the features which cause the secondary maxima in these bands as proposed by Jack et al. (2012). A further, more detailed study of the *R* band is important, since

understanding the detailed composition and ionization structure of the ejecta with time will help to constrain explosion models.

## ACKNOWLEDGEMENTS

We would like to thank the TIGRE team for having made possible the observations of SN 2014J on short notice. We acknowledge with thanks the variable star observations from the AAVSO International Database contributed by observers worldwide and used in this research. We thank Kevin Krisciunas for helpful discussion on the *R*-band light curve. The work has been supported in part by support for programmes HST-GO-122948.04-A provided by NASA through a grant from the Space Telescope Science Institute, which is operated by the Association of Universities for Research in Astronomy, Incorporated, under NASA contract NAS5-26555. This work was also supported in part by the NSF grant AST-0707704. This research used resources of the National Energy Research Scientific Computing Center (NERSC), which is supported by the Office of Science of the US Department of Energy under Contract no. DE-AC02-05CH11231; and the Höchstleistungs Rechenzentrum Nord (HLRN). We thank both these institutions for a generous allocation of computer time.

## REFERENCES

- Amanullah R. et al., 2014, *ApJ*, 788, L21  
 Arnett W. D., 1969, *Ap&SS*, 5, 180  
 Branch D., Doggett J. B., Nomoto K., Thielemann F.-K., 1985, *ApJ*, 294, 619  
 Dessart L., Hillier D. J., 2010, *MNRAS*, 405, 2141  
 Dessart L., Hillier D. J., Blondin S., Khokhlov A., 2014, *MNRAS*, 441, 3249  
 Dilday B. et al., 2012, *Science*, 337, 942  
 Elias J. H., Frogel J. A., Hackwell J. A., Persson S. E., 1981, *ApJ*, 251, L13  
 Fesen R. A., Höflich P. A., Hamilton A. J. S., Hammell M. C., Gerardy C. L., Khokhlov A. M., Wheeler J. C., 2007, *ApJ*, 658, 396  
 Fink M. et al., 2014, *MNRAS*, 438, 1762  
 Foley R. J. et al., 2014, *MNRAS*, 443, 2887  
 Fossey J., Cooke B., Pollack G., Wilde M., Wright T., 2014, *Cent. Bur. Electron. Telegrams*, 3792, 1  
 Gall E. E., Taubenberger S., Kromer M., Sim S. A., Benetti S., Blanc G., Elias-Rosa N., Hillebrandt W., 2012, *MNRAS*, 427, 994  
 Goldhaber G. et al., 2001, *ApJ*, 558, 359  
 Hauschildt P. H., 1992, *J. Quant. Spectrosc. Radiat. Transfer*, 47, 433  
 Hauschildt P. H., Baron E., 1999, *J. Comp. Appl. Math.*, 109, 41  
 Hillebrandt W., Niemeyer J., 2000, *ARA&A*, 38, 191  
 Höflich P., 2003, in Hubeny I., Mihalas D., Werner K., eds, *ASP Conf. Ser. Vol. 288, Stellar Atmosphere Modeling ALI in Rapidly Expanding Envelopes*. Astron. Soc. Pac., San Francisco, p. 185  
 Höflich P., Khokhlov A., Wheeler J. C., 1995, *ApJ*, 444, 831  
 Höflich P., Gerardy C., Fesen R., Sakai S., 2002, *ApJ*, 568, 791  
 Jack D., Hauschildt P. H., Baron E., 2009, *A&A*, 502, 1043  
 Jack D., Hauschildt P. H., Baron E., 2011, *A&A*, 528, A141  
 Jack D., Hauschildt P. H., Baron E., 2012, *A&A*, 538, A132  
 Jack D., Mittag M., Schröder K.-P., Schmitt J., Hempelmann A., González-Pérez J. N., Trinidad M. A., Rauw G., 2015, *MNRAS*, submitted  
 Jordan G. C., Fisher R., Townsley D., Calder A., Graziani C., Asida S., Lamb D., Truran J., 2008, *ApJ*, 681, 1448  
 Jordan G. C., IV, et al., 2012, *ApJ*, 759, 53  
 Kasen D., 2006, *ApJ*, 649, 939  
 Kasen D., Woosley S. E., 2007, *ApJ*, 656, 661  
 Kasen D., Thomas R. C., Nugent P., 2006, *ApJ*, 651, 366  
 Khokhlov A., 1991, *A&A*, 245, 114  
 Khokhlov A., Müller E., Höflich P., 1993, *A&A*, 270, 223  
 Kushnir D., Katz B., Dong S., Livne E., Fernández R., 2013, *ApJ*, 778, L37  
 Levanon N., Soker N., García-Berro E., 2015, *MNRAS*, 447, 2803  
 Long M. et al., 2014, *ApJ*, 789, 103  
 Maeda K., Kutsuna M., Shigeyama T., 2014, *ApJ*, 794, 37  
 Maoz D., Mannucci F., Nelemans G., 2014, *ARA&A*, 52, 107  
 Mazzali P. A., Lucy L. B., 1993, *A&A*, 279, 447  
 Mazzali P. A., Nomoto K., Cappellaro E., Nakamura T., Umeda H., Iwamoto K., 2001, *ApJ*, 547, 988  
 Moll R., Raskin C., Kasen D., Woosley S. E., 2014, *ApJ*, 785, 105  
 Nomoto K., 1984, *ApJ*, 277, 791  
 Nugent P., Phillips M., Baron E., Branch D., Hauschildt P., 1995, *ApJ*, 455, L147  
 Nugent P. E. et al., 2011, *Nature*, 480, 344  
 Pakmor R., Kromer M., Taubenberger S., Sim S. A., Röpke F. K., Hillebrandt W., 2012, *ApJ*, 747, L10  
 Pakmor R., Kromer M., Taubenberger S., Springel V., 2013, *ApJ*, 770, L8  
 Parrent J., Friesen B., Parthasarathy M., 2014, *Ap&SS*, 351, 1  
 Pereira R. et al., 2013, *A&A*, 554, A27  
 Perlmutter S. et al., 1999, *ApJ*, 517, 565  
 Phillips M. M., 1993, *ApJ*, 413, L105  
 Phillips M. M., Lira P., Suntzeff N. B., Schommer R. A., Hamuy M., Maza J., 1999, *AJ*, 118, 1766  
 Pinto P. A., Eastman R. G., 2000a, *ApJ*, 530, 744  
 Pinto P. A., Eastman R. G., 2000b, *ApJ*, 530, 757  
 Pinto P., Eastman R., 2001, *New Astron.*, 6, 307  
 Plewa T., Calder A. C., Lamb D. Q., 2004, *ApJ*, 612, L37  
 Riess A. G., Press W. H., Kirshner R. P., 1996, *ApJ*, 473, 88  
 Riess A. et al., 1998, *AJ*, 116, 1009  
 Rosswog S., Kasen D., Guillochon J., Ramirez-Ruiz E., 2009, *ApJ*, 705, L128  
 Schmitt J. H. M. M. et al., 2014, *Astron. Nachr.*, 335, 787  
 Shigeyama T., Nomoto K., Yamaoka H., Thielemann F.-K., 1992, *ApJ*, 386, L13  
 Sim S. A., Röpke F. K., Hillebrandt W., Kromer M., Pakmor R., Fink M., Ruiter A. J., Seitenzahl I. R., 2010, *ApJ*, 714, L52  
 Sim S. A. et al., 2013, *MNRAS*, 436, 333  
 Wollaeger R. T., van Rossum D. R., 2014, *ApJS*, 214, 28  
 Woosley S. E., Kasen D., 2011, *ApJ*, 734, 38  
 Zheng W. et al., 2014, *ApJ*, 783, L24

This paper has been typeset from a  $\text{\TeX}/\text{\LaTeX}$  file prepared by the author.